

BoSSS: a package for multigrid extended discontinuous Galerkin methods

Florian Kummer and Martin Smuda and Jens Weber

TU Darmstadt, Darmstadt, Germany

Abstract

The software package BoSSS serves the discretization of (steady-state or time-dependent) partial differential equations with discontinuous coefficients and/or time-dependent domains by means of an eXtended Discontinuous Galerkin (XDG, resp. DG) method, aka. cut-cell DG, aka. unfitted DG. This work consists of two major parts: First, the XDG method is introduced and a formal notation is developed, which captures important numerical details such as cell-agglomeration and a multigrid framework. In the second part, iterative solvers for extended DG systems are presented and their performance is evaluated.

Keywords: eXtended Discontinuous Galerkin, cut-cell, unfitted Discontinuous Galerkin, multigrid

1. Introduction and Motivation

BoSSS¹ (*Bounded Support Spectral Solver*) is a flexible framework for the development, evaluation and application of numerical discretization schemes for partial differential equations (PDEs) based on the eXtended Discontinuous Galerkin (XDG) method. The main focus of the XDG method are problems with dynamic interfaces and/or time-dependent domains.

One important field of application for the XDG method are moving geometries: Almost all numerical methods for PDEs require the labor-intensive and thus expensive (semi-manual) creation of numerical grids or meshes. This is particularly cumbersome if time-dependent domains are of interest,

¹ <https://github.com/FDYdarmstadt/BoSSS>

e.g. flows with moving boundaries, as can be found when dealing with a moving geometry (e.g. rotors, pistons but also flexible structures such as heart valves). As a side-product, one could use XDG in order to embed a static geometry, which would be cumbersome to mesh with higher order elements, on a Cartesian background mesh.

A second field of application are multiphase flows, like mixtures of oil and water: due to topology changes, e.g. merging or breakup of droplets, such scenarios would be very difficult to handle with some conformal meshing or mesh-motion techniques like arbitrary Lagrangian-Eulerian (ALE) meshes.

Purpose and scope of this work. All definitions and algorithms found in this paper have their direct counterpart in the source code. However, this work is not intended to be a software manual – in such, the link to the corresponding place in the source code would have to be established with a suitable kind of cross-reference. Since the source code is constantly being developed, the validity of such references would be short-lived.

Instead, this work is intended to serve interested readers as an *axiomatic description of the extended discontinuous Galerkin framework in BoSSS*, in order to assess its capabilities and limitations. We therefore emphasize on issues which are not discussed in publications yet, in specific, details on *multigrid solvers and their performance* will be presented.

1.1. Prototype Problems

Poisson with a jump in coefficients. Let $\Omega \subset \mathbb{R}^D$ ($D \in \{2, 3\}$) be some polygonal domain, which is partitioned into two disjoint but adjacent subdomains \mathfrak{A} and \mathfrak{B} . These might be referred to as *phases*, since they represent e.g. the liquid and gaseous phase in multiphase flow simulations. We assume that the *interface* $\mathfrak{I} := \overline{\mathfrak{A}} \cap \overline{\mathfrak{B}}$ is a $(D - 1)$ - dimensional manifold which is at least \mathcal{C}^1 almost everywhere. Therefore, one can define an oriented normal field $\vec{n}_{\mathfrak{I}}$ on \mathfrak{I} ; w.l.o.g., we assume that $\vec{n}_{\mathfrak{I}}$ “points from \mathfrak{A} to \mathfrak{B} , i.e. $\vec{n}_{\mathfrak{I}}$ is, on \mathfrak{I} , equal to the outer of \mathfrak{A} and an inner normal of \mathfrak{B} . Then, for any property which is continuous in $\Omega \setminus \mathfrak{I}$, one can define the *jump operator*

$$\llbracket f \rrbracket (\vec{x}) := \lim_{\alpha \searrow 0} (f(\vec{x} + \alpha \vec{n}_{\mathfrak{I}}) - f(\vec{x} - \alpha \vec{n}_{\mathfrak{I}})), \quad (1)$$

for $\vec{x} \in \mathcal{I}$. Then, we can define the piece-wise Poisson problem

$$\left\{ \begin{array}{ll} -\mu\Delta u = f & \text{in } \Omega \setminus \mathcal{I}, \\ \llbracket u \rrbracket = 0 & \text{on } \mathcal{I}, \\ \llbracket \mu \nabla u \cdot \vec{n}_{\mathcal{I}} \rrbracket = 0 & \text{on } \mathcal{I}, \\ \vec{u} = g_{\text{Diri}} & \text{on } \Gamma_{\text{Diri}}, \\ \nabla u \cdot \vec{n}_{\partial\Omega} = g_{\text{Neu}} & \text{on } \Gamma_{\text{Neu}}. \end{array} \right. \quad (2)$$

with a discontinuous diffusion coefficient

$$\mu(\vec{x}) = \begin{cases} \mu_{\mathfrak{A}} & \text{for } \vec{x} \in \mathfrak{A}, \\ \mu_{\mathfrak{B}} & \text{for } \vec{x} \in \mathfrak{B}. \end{cases} \quad (3)$$

Incompressible multiphase flows. In a transient setting, the phases are usually considered to be time-dependent too, i.e. one has the decomposition $\Omega = \mathfrak{A}(t) \cup \mathcal{I}(t) \cup \mathfrak{B}(t)$. Using the same notation as introduced above, we introduce the incompressible two-phase Navier-Stokes equation for material interfaces as

$$\left\{ \begin{array}{ll} \partial_t \rho \vec{u} + \text{div}(\rho \vec{u} \otimes \vec{u}) + \nabla p - \text{div}(\mu(\nabla \vec{u} + (\nabla \vec{u})^T)) = -\rho \vec{G} & \text{in } \Omega \setminus \mathcal{I}(t), \\ \text{div}(\vec{u}) = 0 & \text{in } \Omega \setminus \mathcal{I}(t), \\ \llbracket \vec{u} \rrbracket = 0 & \text{on } \mathcal{I}(t) \\ \llbracket p \vec{n}_{\mathcal{I}} - \mu(\nabla \vec{u} + (\nabla \vec{u})^T) \cdot \vec{n}_{\mathcal{I}} \rrbracket = \sigma \kappa \vec{n}_{\mathcal{I}} & \text{on } \mathcal{I}(t), \\ u = \vec{u}_{\text{Diri}} & \text{on } \Gamma_{\text{Diri}}, \\ p \vec{n}_{\mathcal{I}} - \mu(\nabla \vec{u} + (\nabla \vec{u})^T) \cdot \vec{n}_{\mathcal{I}} = 0 & \text{on } \Gamma_{\text{Neu}}. \end{array} \right. \quad (4)$$

with piece-wise constant density and viscosity for both phases, i.e.

$$\rho(\vec{x}) = \begin{cases} \rho_{\mathfrak{A}} & \text{for } \vec{x} \in \mathfrak{A} \\ \rho_{\mathfrak{B}} & \text{for } \vec{x} \in \mathfrak{B} \end{cases} \quad \text{and} \quad \mu(\vec{x}) = \begin{cases} \mu_{\mathfrak{A}} & \text{for } \vec{x} \in \mathfrak{A} \\ \mu_{\mathfrak{B}} & \text{for } \vec{x} \in \mathfrak{B} \end{cases}. \quad (5)$$

Furthermore, σ denotes surface tension and κ denotes the mean curvature of \mathcal{I} . In a two-phase setting, we also assume that the interface does not touches the boundary, i.e. $\mathcal{I}(t) \cap \partial\Omega = \emptyset$. If this is not the case, a three-phase contact line occurs, where two fluids and the solid boundary met at a $D - 2$ – dimensional manifold. This usually requires more sophisticated boundary conditions (see below).

Interface tracking and Level-Set: Note that problem (4) is incomplete without a specification of the interface motion. In order to track the

individual domains, a sufficiently smooth Level-Set field φ is introduced; for sake of simplicity, φ might also be called ‘Level-Set’. Then, time-dependent domains $\mathfrak{A}(t)$, $\mathfrak{B}(t)$ and the interface $\mathfrak{I}(t)$ can be described as

$$\mathfrak{A}(t) := \{ \vec{x} \in \Omega; \varphi(t, \vec{x}) < 0 \}, \quad (6)$$

$$\mathfrak{I}(t) := \{ \vec{x} \in \Omega; \varphi(t, \vec{x}) = 0 \}, \quad (7)$$

$$\mathfrak{B}(t) := \{ \vec{x} \in \Omega; \varphi(t, \vec{x}) > 0 \}. \quad (8)$$

On $\mathfrak{I}(t)$, φ must therefore comply with the Level-Set equation

$$\partial\varphi_t + \nabla\varphi \cdot \vec{u} = 0, \quad (9)$$

which states that the interface speed in normal direction is equal to the flow velocity in normal direction. From the φ , the normal $\vec{n}_{\mathfrak{I}}$ can be computed as

$$\vec{n}_{\mathfrak{I}} = \nabla\varphi / |\nabla\varphi|_2 \quad (10)$$

and the mean curvature can be computed by Bonnets formula as

$$\kappa = \operatorname{div} \left(\frac{\nabla\varphi}{|\nabla\varphi|_2} \right). \quad (11)$$

If the Level-Set is prescribed, e.g. in the case of some externally forced motion, one can infer the interface speed in normal direction from Eq. (9) as

$$s = \frac{-\partial_t\varphi}{|\nabla\varphi|}. \quad (12)$$

Other applications. The XDG framework can be seen as a multi-purpose technology. One obvious application is the use as an immersed boundary method (IBM), e.g. in order to circumvent the (labour-extensive) meshing of domains with complex geometrical details or to represent domains with moving parts. Boundary conditions are weakly enforced at the interface $\mathfrak{I}(t)$ in the same formulation as it would be for boundary fitted methods. The fluid domain is represented by $\mathfrak{A}(t)$, whereas $\mathfrak{B}(t)$ just describes a void region. This was demonstrated for e.g. for moving body flows where the motion of solid particles is characterized by the Newton-Euler equations in the work of Krause and Kummer [1].

Immersed boundaries can also be used in the context of compressible flows. For inviscid flows around immersed boundaries, such as cylinders

and airfoils, Müller et. al. [2] demonstrated the expected high order of convergence for such geometries using an embedded boundary described by a static Level-Set.

A further issue in the scope of multiphase flows (4) is the interaction of the interface with the domain boundary, i.e. the case $\partial\Omega \cap \mathfrak{I}(t) =: \mathfrak{L}(t) \neq \emptyset$: this is referred to as the three-phase contact line between fluids \mathfrak{A} and \mathfrak{B} and the solid. In order to allow motion of the *contact line* $\mathfrak{L}(t)$, the no-slip boundary condition has to be relaxed, yielding the so-called Navier-Slip boundary condition. It is notable that the XDG-implementation does not need further manipulation of the contact line velocity $\vec{U}_{\mathfrak{L}} = (\vec{u} \cdot \vec{n}_{\mathfrak{L}})\vec{n}_{\mathfrak{L}}$ or contact angle Θ . Furthermore, XDG allows the implementation of the generalized Navier-slip boundary condition with

$$\sigma(\cos \Theta_{\text{stat}} - \cos \Theta)\vec{n}_{\mathfrak{L}} = \beta_{\mathfrak{L}}(\vec{u} \cdot \vec{n}_{\mathfrak{L}})\vec{n}_{\mathfrak{L}}, \quad (13)$$

localized at the contact line $\mathfrak{L}(t)$, which is a $D - 2$ - dimensional manifold.

However, for sake of simplicity and moreover, compactness of the presentation, in this work most issues of the XDG method will be discussed with respect to the Poisson problem (2).

1.2. Historical Development and State of the Art

The origins of discontinuous Galerkin (DG) methods can be tracked back to the work of Reed and Hill [3]. The name ‘Discontinuous Galerkin’ was mainly established through the works of Cockburn and Shu [4], although similar methods, based on broken polynomial approximation, ideas were already established earlier: The probably most popular discretization for the Laplace operator, the so-called symmetric interior penalty (SIP) method was proposed by Arnold [5] about nine years earlier.

The idea of adapting a finite element method (FEM) to allow jumps in parameters can be traced back to the 1970s, where Poisson problems with a jump in the diffusion parameter along a smooth interface were investigated by Babuška [6] as well as by Barrett and Elliott [7]. These works mainly relied on isoparametric elements, fitted to the location of the interface at which the discontinuity occurs. Thus, in a transient setting complex motion of the interface is quite difficult to address.

The continuous extended finite element method (XFEM), was presented by Moës et al. [8] to simulate cracking phenomena in solid mechanics. Those ideas were extended to time-dependent problems by Chessa and Belytschko

[9]. The first XFEM for two-phase flows was presented by Groß and Reusken [10, 11]. With the so-called intrinsic XFEM presented by Fries [12], it became possible to represent also kinks in the velocity field. This work was later extended by Cheng and Fries [13] and further by Sauerland and Fries [14]. The first extended DG (XDG) method (also called unfitted DG or cut-cell DG) was presented by Bastian and Engwer [15] in order to model flows in porous media. Later, those approaches were extended to multiphase flows by Heimann et. al. [16].

1.3. The BoSSS code

The development of BoSSS has been initiated at the Chair of Fluid Dynamics in 2008. Since 2017, it is publicly available under the *Apache License*. The very first motivation for BoSSS is to have a suitable code base for the development of XDG methods. Very early, it was decided to investigate both, compressible as well as incompressible flows. The highlights of the code package are:

- XDG and support for flows with dynamic interfaces, which is the main topic of this paper.
- Suitability for High Performance Computing (HPC): All production algorithms in BoSSS are implemented MPI parallel. Furthermore, BoSSS provides instrumentation output in order to analyze and optimize parallel scaling as well as node-level performance. A very important feature is dynamic load balancing, which allows re-distribution of the computational mesh when local processor load changes, e.g. due to motion of the fluid interface.
- Rapid prototyping capability: New models resp. equations can be added in a notation that is close to the usual presentation of DG methods in textbooks, with low development effort. Technical issues, e.g. the handling of the numerical mesh, are provided by the software library.
- Sophisticated workflow and data management facilities: In order to organize and analyze e.g. large parameter studies, database-centric workflow tools were developed.

2. Discontinuous and Extended Discontinuous Galerkin Methods

For sake of completeness, and introducing the notation, we briefly summarize the DG method; The following definitions are fairly standard and can be found in similar form in many textbooks [17, 18].

Definition 1 (basic notations). We define:

- a numerical mesh/grid for Ω is a set $\mathfrak{K}_h = \{K_1, \dots, K_J\}$. The cells are simply connected, cover the whole domain ($\overline{\Omega} = \bigcup_j \overline{K_j}$), but do not overlap ($\int_{K_j \cap K_l} 1 \, dV = 0$ for $l \neq j$).
- the skeleton of the background mesh: $\Gamma := \bigcup_j \partial K_j$. Furthermore, internal edges: $\Gamma_{\text{int}} := \Gamma \setminus \partial\Omega$;
- a normal field \vec{n}_Γ on Γ . On $\partial\Omega$, it represents an outer normal, i.e., on $\partial\Omega$, $\vec{n}_\Gamma = \vec{n}_{\partial\Omega}$. By $\vec{n}_{\mathfrak{I},\Gamma}$, we denote a normal field that is equal to \vec{n}_Γ on Γ and equal to $\vec{n}_{\mathfrak{I}}$ on \mathfrak{I} ;

For sake of completeness, we notate the approximation space of the ‘standard’ DG method:

Definition 2 (DG space). The broken polynomial space of total degree k is defined as:

$$\mathbb{P}_k(\mathfrak{K}_h) := \{f \in L^2(\Omega); \forall K \in \mathfrak{K}_h : f|_K \text{ is polynomial and } \deg(f|_K) \leq k\}; \quad (14)$$

2.1. Extended Discontinuous Galerkin and Level-Set

In order to yield a well-defined interface \mathfrak{I} , the Level-Set-field $\varphi(t, -)$ must be sufficiently smooth. Precisely, we assume $\varphi(t, -)$ to be almost-everywhere in $\mathcal{C}^1(\Omega)$. For certain steady-state problems with simple interface shapes, one can represent φ by an explicit formula that can e.g. be inserted into to code directly. In more complicated cases, or for temporally evolving problems, φ may be itself a continuous broken polynomial on the background mesh, i.e. $\varphi(t, -) \in \mathcal{C}^0(\Omega) \cap \mathbb{P}_k(\mathfrak{K}_h)$. In both cases, one can infer an interface normal (Eq. 10) as well as the interface speed (Eq 12) from φ .

Definition 3 (Cut-cell mesh). Time-dependent cut-cells are given as

$$K_{j,\mathfrak{A}}(t) := K_j \cap \mathfrak{A}(t), \quad K_{j,\mathfrak{B}}(t) := K_j \cap \mathfrak{B}(t). \quad (15)$$

The set of all cut-cells form the *time-dependent cut-cell mesh* $\mathfrak{K}_h^X(t)$.

Note that we refer to the ‘original cells’ K_j as *background cells*, in contrast to the time-dependent cut-cells $K_{j,s}(t)$. By \mathfrak{s} , resp. $\mathfrak{s}(t)$ a notation for an arbitrary phase is introduced, i.e. \mathfrak{s} can be either \mathfrak{A} or \mathfrak{B} .

XDG is essentially a DG method on cut-cells, i.e. one can define the XDG space as follows:

Definition 4 (XDG space). We define:

$$\mathbb{P}_k^X(\mathfrak{K}_h, t) := \mathbb{P}_k(\mathfrak{K}_h^X(t)) \quad (16)$$

Most DG methods are written in terms of jump- and average operators, as already defined on \mathfrak{J} , see Eq. (1). This notation is extended onto the skeleton of the mesh Γ :

Definition 5 (inner and outer value, jump and average operator). At the mesh skeleton, the inner- resp. outer-value of a field $u \in \mathcal{C}^0(\Omega \setminus \Gamma_{\text{int}} \setminus \mathfrak{J})$ are defined as:

$$\begin{aligned} u^{\text{in}}(\vec{x}) &:= \lim_{\xi \searrow 0} u(\vec{x} - \xi \vec{n}_{\mathfrak{J},\Gamma}) \quad \text{for } \vec{x} \in \Gamma \cup \mathfrak{J} \\ u^{\text{out}}(\vec{x}) &:= \lim_{\xi \searrow 0} u(\vec{x} + \xi \vec{n}_{\mathfrak{J},\Gamma}) \quad \text{for } \vec{x} \in \Gamma_{\text{int}} \cup \mathfrak{J} \end{aligned}$$

Then, the jump and average value operator are defined as

$$\llbracket u \rrbracket := \begin{cases} u^{\text{in}} - u^{\text{out}} & \text{on } \Gamma_{\text{int}} \\ u^{\text{in}} & \text{on } \partial\Omega \end{cases}, \quad (17)$$

$$\{\{u\}\} := \begin{cases} (u^{\text{in}} + u^{\text{out}})/2 & \text{on } \Gamma_{\text{int}} \\ u^{\text{in}} & \text{on } \partial\Omega \end{cases}. \quad (18)$$

For the implementation of an XDG-method, accurate numerical integration on the cut-cells $K_{j,s}(t)$ is required. In BoSSS the user can either select the Hierarchical Moment Fitting (HMF) procedure, developed by Müller et al. [19], or, alternatively, a method proposed by Saye [20]. While the HMF supports all types of cells (triangles, quadrilaterals, tetra- and hexahedrons) the method of Saye is generally faster, but restricted to quadrilaterals and hexahedrons.

Ensuring continuity of φ , computation of normals and curvature. Some XDG method for the two-phase Navier Stokes problem (4) has to be coupled with a second method to compute the evolution of the interface. Since the respective Level-Set equation (9) is of hyperbolic type, a conventional DG approximation seems a reasonable choice. However, such a method will typically yield a

discontinuous field φ . In such cases, φ needs to be projected to a continuous space before it can be used to setup the XDG method. Furthermore, the curvature κ required in problem (4), see also Eq. (11), needs to be handled with care. For a detailed presentation of the filtering procedures used in BoSSS, we refer to the work of Kummer and Warburton [21]. For sake of simplicity, in this work we assume φ to be sufficiently smooth with respect to space and time.

2.2. Variational formulations

Now, problems (2) and (4) can be discretized in the XDG space. In general, we are interested in systems like the Navier-Stokes equation, with D_v dependent variables which are not necessarily discretized with the same polynomial degree. We therefore define the degree-vector $\underline{k} = (k_1, \dots, k_{D_v})$; and introduce an abbreviation for the function space of test and trial functions,

$$\mathbb{V}_{\underline{k}}^X(t) := \prod_{\gamma=1}^{D_v} \mathbb{P}_{k_\gamma}^X(\mathfrak{K}_h, t). \quad (19)$$

Then, the discrete version of some linear problem, for a fixed time t formally read as: find $U \in \mathbb{V}_{\underline{k}}^X(t)$ so that

$$a(U, V) = b(V) \quad \forall V \in \mathbb{V}_{\underline{k}}^X(t). \quad (20)$$

Discrete variational formulation for Poisson Eq. (2). The variational formulation of the symmetric interior penalty method, originally proposed by Arnold [5], reads as

$$\begin{aligned} a_{\text{sip}}(u, v) := & - \oint_{\mathfrak{J} \cup \Gamma \setminus \Gamma_{\text{Neu}}} \{ \{ \mu \nabla_h u \} \} \cdot \vec{n}_{\mathfrak{J}, \Gamma} \llbracket v \rrbracket + \{ \{ \mu \nabla_h v \} \} \cdot \vec{n}_{\mathfrak{J}, \Gamma} \llbracket u \rrbracket \, dS \\ & + \oint_{\mathfrak{J} \cup \Gamma \setminus \Gamma_{\text{Neu}}} \eta \max\{\mu^{\text{in}}, \mu^{\text{out}}\} \llbracket u \rrbracket \llbracket v \rrbracket \, dS + \int_{\Omega} \mu \nabla_h u \cdot \nabla_h v \, dV \end{aligned} \quad (21)$$

for the left-hand-side of Eq. (20). Here, $\nabla_h u$ denotes the broken gradient, where differentiation at the jumps on $\Gamma \cup \mathfrak{J}$ is excluded. The linear form on the right-hand-side of Eq. (20) is given as

$$b(v) := \int_{\Omega} f v \, dV - \oint_{\Gamma_{\text{Diri}}} \mu g_{\text{Diri}} (\nabla_h v \cdot \vec{n}_{\partial\Omega} - \eta v) \, dS + \oint_{\Gamma_{\text{Neu}}} \mu g_{\text{Neu}} v \, dS \quad (22)$$

The SIP factor η is known to scale as $\eta \approx \text{const} \cdot k^2/h'$, where h' is a local length scale of the agglomerated cut-cell, see section 2.3. For certain specific cell shapes, explicit formulas for η can be given, a comprehensive overview is given in the thesis of Hillewaert [22]. In the case of XDG methods with arbitrary cell shapes, some rules-of-thumb can be used, given that a sufficiently large multiplicative constant is used. Alternatively, a symmetric weighted interior penalty (SWIP) form, as presented in the textbook of Di Pietro & Ern [17] might be used.

Discrete variational formulation for Navier-Stokes Eq. (4). Due to the non-linearity in the convective term, the Navier-Stokes system is usually split up into the linear Stokes part $a(-, -)$ and the nonlinear convection operator $c(-, -, -)$. It is known that, in order to obtain an inf-sup stable discretization, the DG polynomial degree of the pressure has to be one lower than for velocity, i.e. velocity is discretized with degree k and pressure with degree $k - 1$. (Note this is proven only for special cases, see the work of Girault et. al. [23].) In this notational framework, for spatial dimension $D = 3$, we write $D_v = D + 1$ and $\underline{k} = (k, \dots, k, k - 1)$. The variational formulation of the Navier-Stokes equation formally reads as: find $U = (\vec{u}, p) \in \mathbb{V}_{\underline{k}}^X(t) = (\mathbb{P}_k^X(\mathfrak{R}_h, t))^D \times \mathbb{P}_{k-1}^X(\mathfrak{R}_h, t)$ so that

$$\int_{\Omega} \partial_t U \cdot V \, dV + c(U, U, V) + a(U, V) = b(V) \quad \forall V \in \mathbb{V}_{\underline{k}}^X(t). \quad (23)$$

A complete specification of the involved forms would be too lengthy here; hence, we refer to the works of Heimann et. al. [16] and Kummer [24]. Obviously, (i) this equation still requires a temporal discretization and (ii) a nonlinear solver.

For sake of simplicity, we assume an implicit Euler discretization in time, i.e. $\partial_t U \approx (U^1 - U^0)/\Delta t$, where $U^0 \in \mathbb{V}_{\underline{k}}^X(t^0)$ denotes the known value from previous timestep t^0 , and $U^1 \in \mathbb{V}_{\underline{k}}^X(t^1)$ denotes the unknown value at the new timestep t^1 , i.e. $t^1 - t^0 = \Delta t$. We also fix the first argument of $c(-, -, -)$. Then, scheme (23) reduces to a form which is formally equivalent to scheme (20), namely: find $U^1 \in \mathbb{V}_{\underline{k}}^X(t^1)$ so that

$$\int_{\Omega} U^1 \cdot V \, dV + c(U_0, U^1, V) + a(U^1, V) = b(V) + \int_{\Omega} U^0 \cdot \mathcal{L}_{t^1}^{t^0} V \, dV \quad \forall V \in \mathbb{V}_{\underline{k}}^X(t^1). \quad (24)$$

The linearization point U_0 may be either set as $U_0 = U^0$, which results in a semi-implicit formulation. Alternatively, one can utilize fully implicit approach and iterate over equation (24), so that $U_0 \rightarrow U^1$ or employ a Newton method.

On the right-hand-side, the linear operator $\mathcal{L}_{t^1}^{t^0}$ performs a lifting from $\mathbb{V}_k^X(t^1)$ to $\mathbb{V}_k^X(t^0)$. This requires that the corresponding part of the right-hand-side of (24) must be integrated on the old cut-cell mesh at time t^0 .

The lifting is defined as follows:

Definition 6 (temporal XDG space lifting). The cut-cell mesh $\mathfrak{K}_h^X(t^0)$ and $\mathfrak{K}_h^X(t^1)$ at times t^0 and t^1 have equal topology, if, and only if for each cut-cell one has

$$\begin{aligned} |K_{j,\mathfrak{s}}(t^0)| > 0 &\quad \Rightarrow \quad |K_{j,\mathfrak{s}}(t^0) \cap K_{j,\mathfrak{s}}(t^1)| > 0 \text{ and} \\ |K_{j,\mathfrak{s}}(t^1)| > 0 &\quad \Rightarrow \quad |K_{j,\mathfrak{s}}(t^1) \cap K_{j,\mathfrak{s}}(t^0)| > 0. \end{aligned}$$

On meshes with equal topology, the lifting operator

$$\mathbb{P}_k^X(\mathfrak{K}_h, t^1) \ni u^1 \mapsto \mathcal{L}_{t^1}^{t^0} u^1 =: u^0 \in \mathbb{P}_k^X(\mathfrak{K}_h, t^0)$$

is uniquely defined requiring polynomial equality on the common domain of old and new cut-cell, i.e. by the property

$$u^0|_{K_{j,\mathfrak{s}}(t^0) \cap K_{j,\mathfrak{s}}(t^1)} = u^1|_{K_{j,\mathfrak{s}}(t^0) \cap K_{j,\mathfrak{s}}(t^1)} \quad \forall j, \mathfrak{s}.$$

Since $\mathbb{V}_k^X(t)$ is a product of spaces $\mathbb{P}_k^X(\mathfrak{K}_h, t)$, the lifting $\mathcal{L}_{t^1}^{t^0} u^1$ naturally extends to $\mathbb{V}_k^X(t)$. Obviously, it cannot always be ensured that the cut-cell meshes for t^0 and t^1 have equal topology. However, this important property can be achieved through cell agglomeration, which is addressed in the next section.

2.3. Cell agglomeration

The motivation for aggregation/agglomeration meshes is three-fold: removal of small cut-cells, avoiding topology changes in the cut-cell mesh for a single time-step and formulation of multigrid methods without the usual hierarchy of meshes, cf. Section 3 and Figure 1).

Formally, the aggregation mesh is introduced by means of graph theory:

Definition 7 (Graph of a numerical mesh). Let \mathfrak{K} be a numerical mesh; For $K_1, K_2 \in \mathfrak{K}$, the set $\{K_1, K_2\}$ is called a *logical edge* if, and only if $\int_{\overline{K_1 \cap K_2}} 1 \, dS > 0$. Furthermore, let $Edg(\mathfrak{K})$ be the set of all logical edges. Then, the pair $(\mathfrak{K}, Edg(\mathfrak{K})) =: Gr(\mathfrak{K})$ forms an undirected graph in the usual sense.

Definition 8 (Aggregation maps and meshes). Let $A \subset Edg(\mathfrak{K})$ be an aggregation map and $a := \{K_1, \dots, K_L\}$ be the nodes of a connected component of $Gr(\mathfrak{K})$. Note that a might consist of only a single element, i.e. an isolated node, which is called a non-aggregated cell with respect to A . The aggregate cell is defined as the union of all cells, i.e. $K_a := \bigcup_{K_l \in a} K_l$ (Rem.: in order to ensure that the aggregate cell is again a simply connected, open set, one has to take the closure of each cell first and then subtract the boundary, therefore we define a modified union as $X \cup^\partial Y := (\overline{X} \cup \overline{Y}) \setminus \partial(\overline{X} \cup \overline{Y})$.)

For $A \subset Edg(\mathfrak{K})$ the aggregation mesh $Agg(\mathfrak{K}_h, A)$ is the set of all aggregate cells which can be formed w.r.t. A .

Based upon the aggregation mesh, an aggregated XDG space can be defined:

Definition 9 (Aggregated XDG space). For some agglomeration map $A \in Edg(\mathfrak{K}_h^X(t^1))$ we define the agglomerated XDG space as:

$$\mathbb{P}_k^{X^A}(\mathfrak{K}_h, t) := \mathbb{P}_k(Agg(\mathfrak{K}_h^X(t), A)) \quad (25)$$

Obviously, the agglomerated XDG space is a sub-space of the original space, i.e. $\mathbb{P}_k^{X^A}(\mathfrak{K}_h, t) \leq_{\mathbb{R}} \mathbb{P}_k^X(\mathfrak{K}_h, t)$.

Temporal discretization and stabilization against small cut-cells. As already noted above, in order to discretize temporally evolving systems such as Eq. (24), one has to ensure that the cut-cell mesh at time steps t^0 and t^1 have equal topology in order to obtain a well-defined method. Otherwise, the required lifting operator (see Definition 6) is undefined. For multi-step schemes, which involve multiple time steps, the topology has to be equal for all time steps; the same holds for the intermediate steps of Runge-Kutta schemes, cf. [25].

Furthermore, since the interface position is arbitrary, cut-cells can be arbitrarily small, i.e. its volume fraction $|K_{j,s}(t)|/|K_j|$ w.r.t. the background cell can be small. This leads e.g. to large penalty parameters η in the SIP

form (21) which is known to cause undesirably high condition numbers of the discretized system.

Therefore, instead of solving the variational system on the space $\mathbb{V}_{\underline{k}}^X(t)$, which is induced by the cut-cell mesh, one employs an XDG space on an appropriately agglomerated cut-cell mesh. A valid agglomeration map $A_{\alpha,t^1,t^0} \subset \text{Edg}(\mathfrak{R}_h^X(t^1)) \cup \text{Edg}(\mathfrak{R}_h^X(t^0))$ for these purpose must meet the following requirements:

- The meshes $\text{Agg}(\mathfrak{R}_h^X(t^1), A_{\alpha,t^1,t^0})$ and $\text{Agg}(\mathfrak{R}_h^X(t^0), A_{\alpha,t^1,t^0})$ have the same topology.
- All cut-cells with a volume fraction $0 < |K_{j,s}(t)|/|K_j| \leq \alpha$ are agglomerated
- There is no agglomeration across species, i.e. there exists no edge $\{K_{j,\mathfrak{A}}, K_{l,\mathfrak{B}}\}$ in A_{α,t^1,t^0} .

The formulation of an algorithm that constructs an agglomeration map which fulfills the properties noted above is left to the reader. It may consist of a loop over all cut-cells. The cut-cell $K_{j,s}$ must be agglomerated if it is a new cell (i.e. $|K_{j,s}(t^1)| > 0$ and $|K_{j,s}(t^0)| = 0$) or a vanished cell (i.e. $|K_{j,s}(t^1)| = 0$ and $|K_{j,s}(t^0)| > 0$) or if its volume fraction is below the threshold α . A decent value for α lies in the range of 0.1 to 0.3, cf. [24, 2]. In our implementation, such a cell is agglomerated to its largest neighbor cell in the same species.

The final system. Instead of solving the generic variational system (20) on the space $\mathbb{V}_{\underline{k}}^X(t^1)$, the aggregated space

$$\mathbb{V}_{\underline{k}}^{X,\alpha,\Delta t} := \prod_{\gamma=1}^{D_v} \mathbb{P}_k^{X A_{\alpha,t^0,t^1}}(\mathfrak{R}_h, t^1) \quad (26)$$

is used for discretization. In comparison to (19), the dependence on time t is dropped since w.l.o.g. all temporally evolving systems are solved for the ‘new’ time step t^1 .

Hence, the final discretization reads as: find $U \in \mathbb{V}_{\underline{k}}^{X,\alpha,\Delta t}$ so that

$$a(U, V) = b(V) \quad \forall V \in \mathbb{V}_{\underline{k}}^{X,\alpha,\Delta t}. \quad (27)$$

Over the course of multiple time-steps, the agglomeration graph typically changes. After each time step is complete, the solution is injected into the

non-agglomerated space. For the next time step it is projected back (in an L^2 -sense) onto the (potentially different) agglomerated space to serve as an initial value.

3. Multigrid solvers

The remaining of this paper is dedicated to the solution of the linear system (27). The solvers presented are use a combination of aggregation- and p-multigrid. Aggregation multigrid can be seen as a combination of conventional h-multigrid and algebraic multigrid methods: there is still an underlying mesh of polyhedral cells. Due to these cells, the flexibility is comparable to algebraic multigrid, see Figure 1.

This section is organized as follows: first, the aggregation multigrid framework will be unified with the XDG method established so far (section 3.1). Next, the construction of a basis for the nested sequence of approximation spaces will be laid out, in order to transfer the basis-free formulation (27) into a matrix form. Finally, the specific combination of multigrid algorithms are presented (3.3).

3.1. Aggregation multigrid for XDG

The starting point of the aggregation multigrid is a sequence of aggregation maps

$$\emptyset = A^1 \subset A^2 \subset \dots \subset A^\Lambda \subset \text{Edg}(\mathfrak{R}_h) \quad (28)$$

on the background mesh. Note that the injection/projection operator between aggregation grid are quite expensive to compute. Therefore, it is beneficial to compute them initially and only update when necessary in cut-cells. Since these are defined on the background mesh, in order to be precomputed, one cannot directly apply these aggregation maps onto the cut-cell mesh. Therefore, aggregation maps from the background mesh must be mapped onto the cut-cell mesh:

Definition 10 (Mapping of an aggregation map onto a cut-cell mesh). Given is an aggregation map $A \subset \text{Edg}(\mathfrak{R}_h)$ on the background mesh \mathfrak{R}_h . The corresponding aggregation map $A^X(t)$ on the cut-cell mesh $\mathfrak{R}_h^X(t)$ is formed from all edges $\{K_j, K_l\} \in A$ by duplicating them for each species, i.e. from edges

$$\{K_{j,s}(t), K_{l,s}(t)\} \quad \forall s \in \{\mathfrak{A}, \mathfrak{B}\}, \text{ if } |K_{j,s}(t)| > 0 \text{ and } |K_{l,s}(t)| > 0.$$

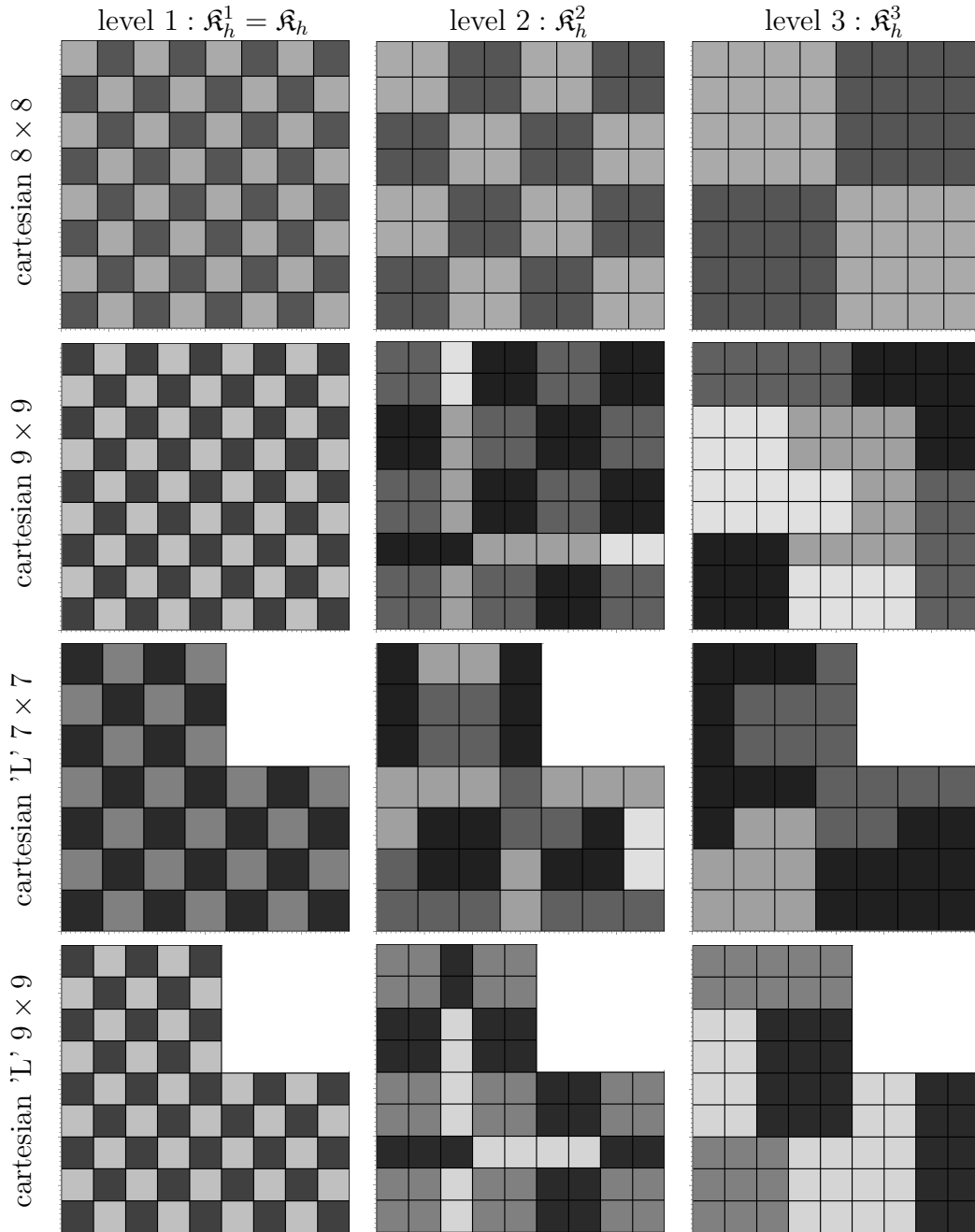


Figure 1: Examples of aggregation multigrid: an advantage of this approach is that it is with respect to geometry more flexible than the classical geometric multigrid approach where the finest grid level is induced by the coarsest.

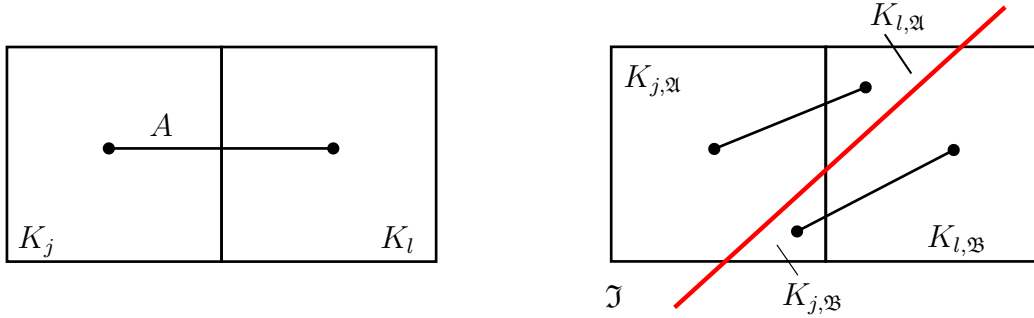


Figure 2: From an aggregation map $A \subset \text{Edg}(\mathfrak{K}_h)$ (left) to the corresponding map $A^X(t) \subset \text{Edg}(\mathfrak{K}_h^X(t))$ on the cut-cell mesh (right). Since the edges of A are duplicated for each species, no aggregation across the interface \mathfrak{J} occurs.

Note that this construction avoids aggregation across the interface \mathfrak{J} , as illustrated in Figure 2. Through the mapping of an aggregation map $A \mapsto A^X(t)$, a sequence of aggregated XDG spaces is induced,

$$\mathbb{V}_{\underline{k}}^{X,\alpha,\Delta t} =: \mathbb{V}_{\underline{k}}^{X,1} \mathbb{R} \geq \mathbb{V}_{\underline{k}}^{X,2} \mathbb{R} \geq \cdots \mathbb{R} \geq \mathbb{V}_{\underline{k}}^{X,\Lambda}$$

where the space on mesh level λ can be defined as

$$\mathbb{V}_{\underline{k}}^{X,\lambda} := \prod_{\gamma=1}^{D_v} \mathbb{P}_{\underline{k}}^{X,A'^\lambda}(\mathfrak{K}_h, t^1) \quad (29)$$

and the aggregation map is the union of the predefined multigrid aggregation sequence (see 28) and the aggregation map A_{α,t^1,t^0} to stabilize small cut-cells and prevent temporal topology changes, i.e.

$$A'^\lambda := (A^\lambda)^X(t^1) \cup A_{\alpha,t^1,t^0}. \quad (30)$$

3.2. Basis representation and indexing

Up to this point, the XDG method is formulated in a variational, coordinate-free form. In order to notate solver algorithms in a typical matrix-notation, a basis representation of the XDG space is required.

A Basis of $\mathbb{V}_{\underline{k}}^{X,\lambda}$. The elements of the basis are written as $\vec{\Phi}_{j,\gamma,s,n}^\lambda$, with the following index conventions:

- $j \in \mathbb{J}^\lambda$ is the index related to the background cell, where for aggregation cells one picks the minimum cell index of all aggregated background cells on mesh level 0 as a representative,

- γ is the variable index (e.g. for Navier-Stokes, $1 \leq \gamma \leq D$ corresponds to the velocity components and $\gamma = D + 1$ corresponds to pressure),
- $\mathfrak{s} \in \{\mathfrak{A}, \mathfrak{B}\}$ is the species index and
- $1 \leq n \leq N_{k\gamma}$ is the DG-mode index, where N_k is the dimension of the polynomial space up to degree k .

The row-vector of all XDG basis functions, on mesh level λ is written as

$$\left(\bar{\Phi}_{j,\gamma,\mathfrak{s},n}^{X,\lambda} \right)_{j,\gamma,\mathfrak{s},n} =: \underline{\underline{\Phi}}^{X,\lambda}. \quad (31)$$

(Here, we skik the specification of all valid combinations of $j, \gamma, \mathfrak{s}, n$ for sake of compactness.) In the implementation, this basis is constructed from a basis $\underline{\Phi} = (\Phi_{j,n})_{\substack{j=1,\dots,J \\ n=1,\dots,N_k}}$ on the space $\mathbb{P}_k(\mathfrak{R}_h)$, with $\text{supp}(\Phi_{j,n}) = K_j$ in the following way: first, a basis $\underline{\Phi}^\lambda$ of the aggregated space $\mathbb{P}_k(\text{Agg}(\mathfrak{R}_h, A^\lambda))$ is created. Since $\mathbb{P}_k(\text{Agg}(\mathfrak{R}_h, A^\lambda)) \leq_{\mathbb{R}} \mathbb{P}_k(\mathfrak{R}_h)$, one can express this basis in terms of the original basis, i.e.

$$\underline{\Phi}^\lambda = \underline{\Phi} \cdot \underline{\underline{Q}}^\lambda,$$

with a suitable matrix $\underline{\underline{Q}}$. It can be derived from an Ansatz which projects a polynomial basis on the bounding box of an aggregation cell onto the background cells, for details see ref. [24].

The matrix $\underline{\underline{Q}}^\lambda$ obviously is a prolongation operator. If both, $\underline{\Phi}^\lambda$ and $\underline{\Phi}$ are orthonormal, the mapping

$$\mathbb{P}_k(\mathfrak{R}_h) \ni \underline{\Phi} \cdot \underline{u} \mapsto \underline{\Phi}^\lambda \cdot ((\underline{\underline{Q}}^\lambda)^T \underline{u}) \in \mathbb{P}_k(\text{Agg}(\mathfrak{R}_h, A^\lambda))$$

is a projector in the L^2 -sense.

For computational efficiency and in order to save memory, the matrix $\underline{\underline{Q}}$ should not be stored. Instead, $\underline{\Phi}^{\lambda+1}$ is expressed in terms of $\underline{\Phi}^\lambda$, i.e.

$$\underline{\Phi}^{\lambda+1} = \underline{\Phi}^\lambda \cdot \underline{\underline{R}}^\lambda. \quad (32)$$

For orthonormal bases, $\underline{\underline{R}}^\lambda$ is the prolongation matrix from the coarse to fine mesh, while $(\underline{\underline{R}}^\lambda)^T$ is a restriction, resp. projection matrix from fine to coarse mesh. For a specific aggregation cell, it can be computed by projection

of polynomials onto one representative background cell for each part of the aggregation cell.

Second, the basis of the XDG space is constructed: the basis elements of $\mathbb{V}_{\underline{k}}^{X,\lambda}$ are expressed as

$$\vec{\Phi}_{j,\gamma,\mathfrak{s},n}^{X,\lambda}(\vec{x}) := \vec{e}_\gamma \sum_{m=1}^{N_{k_\gamma}} \Phi_{j,m}^\lambda(\vec{x}) \chi_{\mathfrak{s}(t)}(\vec{x}) S_{mn}^\lambda. \quad (33)$$

Here \vec{e}_γ is the standard basis vector in \mathbb{R}^{D_v} and $\chi_{\mathfrak{s}}$ denotes the characteristic function for set \mathfrak{s} . The matrix $\underline{\underline{S}}^\lambda$ provides a re-orthonormalization of the basis functions $\Phi_{j,m}^\lambda \chi_{\mathfrak{s}(t)}$ in cut-cells and can be obtained e.g. through a Cholesky factorization.

Finally, through a combination of multigrid projection matrices $\underline{\underline{R}}^\lambda$ and re-orthonormalization matrices $\underline{\underline{S}}^\lambda$, one obtains the representation

$$\underline{\underline{\Phi}}^{X,\lambda+1} = \underline{\underline{\Phi}}^{X,\lambda} \cdot \underline{\underline{R}}^{X,\lambda}. \quad (34)$$

Formally, $\underline{\underline{R}}^{X,\lambda}$ is a matrix product of $\underline{\underline{S}}^\lambda$ and $\underline{\underline{R}}^\lambda$. The notation of its exact shape is rather technical and therefore skipped. Mainly, since e.g. $\underline{\underline{\Phi}}^{X,\lambda}$ are vector-valued an advanced indexing notation is required, which is introduced below.

Multi-index mapping. In order to extract sub-matrices and sub-vectors which correspond to certain cells, variables and DG modes, a sophisticated index notation is required. A single basis element of $\mathbb{V}_{\underline{k}}^{X,\lambda}$ can be associated with a multi-index $m(j, \gamma, \mathfrak{s}, n)$. One may think of $m(-, -, -, -)$ as a bijection between all valid combinations of j , γ , \mathfrak{s} and n and the set $I := \{1, \dots, \dim(\mathbb{V}_{\underline{k}}^{X,\lambda})\}$. We use a notation where the mapping $m(-, -, -, -)$ is employed to select sub-sets of I , e.g.

$$m(j, -, -, \leq N_{\underline{k}}) := \{m(j, d_v, \mathfrak{s}, n); \forall d_v, \forall \mathfrak{s} \text{ present in cell } j, \forall n \leq N_{k_{d_v}}\}.$$

Such sets will be used to notate sub-matrices or sub-vectors, similar to the typical MATLAB notation.

Agglomeration Algebra. Given that a basis is established, the generic system (27) which searches for a solution $U \in \mathbb{V}_{\underline{k}}^{X,\lambda}$ can be transferred to an equivalent matrix formulation

$$\underline{\underline{M}}^\lambda \underline{\underline{U}} = \underline{\underline{b}}^\lambda \quad (35)$$

with

$$M_{m(j,d_v,s,n) \ m(l,e_v,r,m)}^\lambda = a(\vec{\Phi}_{l,e_v,r,m}^{X,\lambda}, \vec{\Phi}_{j,d_v,s,n}^{X,\lambda}) \text{ and } b_{m(j,d_v,s,n)}^\lambda = b(\vec{\Phi}_{l,e_v,r,m}^{X,\lambda}). \quad (36)$$

Through restriction and prolongation matrices, one obtains the relation

$$\underline{\underline{M}}^{\lambda+1} = (\underline{\underline{R}}^{X,\lambda})^T \underline{\underline{M}}^\lambda \underline{\underline{R}}^{X,\lambda} \text{ and } \underline{\underline{b}}^{\lambda+1} = (\underline{\underline{R}}^{X,\lambda})^T \underline{\underline{R}}^\lambda, \quad (37)$$

as usual in multigrid methods.

3.3. Preconditioners and Solvers

Within this section the discussion is focused on a single mesh level λ , hence the level index is dropped. On this grid level, let L be the vector space dimension, i.e. $\underline{\underline{M}} = \underline{\underline{M}}^\lambda \in \mathbb{R}^{L \times L}$. The (approximate) solution and right-hand-side (RHS) vector of the system (35) are denoted as $\underline{\underline{x}}, \underline{\underline{b}} \in \mathbb{R}^L$, respectively.

In this section, a series of algorithms is introduced.

- A p-multigrid algorithm (Algorithm 11), that operates on a single mesh level, which can be used as a pre-conditioner for a standard GMRES solver.
- The additive Schwarz algorithm (Algorithm 12), which uses p-multigrid as a block solver. It contains a minor modification to its original form, which we found helpful in decreasing the number of iterations and is therefore also presented here.
- Finally, the orthonormalization multigrid algorithm (Algorithm 14) which employs the additive Schwarz as a smoother and a residual minimization (Algorithm 13) to ensure non-increasing residual norms.

A p-multigrid pre-conditioner on a single mesh level. For DG or XDG methods, even without aggregation meshes, a p-multigrid seems to be a reasonable idea: At first, a sub-matrix which corresponds to low order DG modes is extracted. Since the number of degrees-of-freedom for this is typically low, a sparse direct solver can be used. The degrees of freedom which correspond to higher order DG modes are then solved locally in each cell. Since Algorithm 11 will also be used as a block solver for the additive Schwarz method (Algorithm 12), an optional index-set $\mathbb{I} \subset \mathbb{J}^\lambda$ which restricts the solution to a part of the mesh can be provided.

Algorithm 11 (p-multigrid pre-conditioner). $\underline{x} = \text{PMG}(\underline{b}, \underline{k}_{\text{lo}}, \mathbb{I})$ is computed as follows:

Input: A right-hand-side \underline{b} , a vector of DG polynomial degrees $\underline{k}_{\text{lo}}$ which separates low from high order modes, for each variable. Optionally, an index-set $\mathbb{I} \subset \mathbb{J}^\lambda$ of sub-cells, denoting the block to solve.

Output: An approximate solution \underline{x}

$\underline{x} := 0$	▷ initialize approximate solution
$I_{\text{lo}} := m(\mathbb{I}, -, -, \leq N_{\underline{k}_{\text{lo}}})$	▷ Indices for low-order modes in cells \mathbb{I}
$\underline{\underline{M}}_{\text{lo}} := \underline{\underline{M}}_{I_{\text{lo}}, I_{\text{lo}}}$	▷ extract low-order system
$\underline{b}_{\text{lo}} := \underline{b}_{I_{\text{lo}}}$	▷ extract low-order RHS
Solve: $\underline{x}_{\text{lo}} := \underline{\underline{M}}_{\text{lo}} \setminus \underline{b}_{\text{lo}}$	▷ usually using a sparse direct solver
$\underline{x}_{I_{\text{lo}}} := \underline{x}_{I_{\text{lo}}} + \underline{x}_{\text{lo}}$	▷ accumulate low-order solution
$\underline{r} := \underline{b} - \underline{\underline{M}}\underline{x}$	
for all $j \in \mathbb{I}$ do	▷ loop over cells...
$I_{\text{hi},j} := m(j, -, -, > N_{\underline{k}_{\text{lo}}})$	▷ Indices for high-order modes in cell j
$\underline{\underline{M}}_{\text{hi},j} := \underline{\underline{M}}_{I_{\text{hi},j}, I_{\text{hi},j}}$	▷ extract high-order system in cell j
$\underline{b}_{\text{hi},j} := \underline{b}_{I_{\text{hi},j}}$	▷ extract high-order RHS in cell j
Solve: $\underline{x}_{\text{hi},j} := \underline{\underline{M}}_{\text{hi},j} \setminus \underline{b}_{\text{hi},j}$	▷ using a dense direct solver
$\underline{x}_{I_{\text{hi},j}} := \underline{x}_{I_{\text{hi},j}} + \underline{x}_{\text{hi},j}$	▷ accumulate local high-order solution
end for	

Since a preconditioner typically has to be applied multiple time, it is essential for performance to use a sparse direct solver for the low order system which is able to store the factorization and apply multiple right-hand sides. Numerical tests hint that usually a single-precision solvers is sufficient as long as the residuals are computed in double precision. The PMG algorithm presented above can directly be used as a preconditioner, e.g. for GMRES. However, since only two multigrid levels are used, its application typically is only reasonable up to medium-sized systems.

An additive Schwarz method. In the scope of this work, $\text{PMG}(\dots)$ is also used as a block solver for an additive Schwarz method. For a general discussion on Schwarz methods, we refer to the review article of Gander [26]. In our implementation the blocking is determined on the level of cells, i.e. on the basis of the mesh \mathfrak{R}_h^λ . The METIS [27] software library is used to partition \mathfrak{R}_h^λ ; the number of partitions is determined so that a single partition contains roughly 10,000 degrees-of-freedom. After the partitioning by METIS, each

partition is enlarged by its neighbor cells to generate the overlap layer that is typically used with Schwarz methods.

Algorithm 12 (Additive Schwarz). $\underline{x} = \text{Swz}(\underline{b})$ is computed as follows:

Input: A right-hand-side \underline{b} , a vector of DG polynomial degrees $\underline{k}_{\text{lo}}$ which separates low from high order modes, for each variable. Furthermore, a pre-computed partitioning of cells, i.e. sets $\mathbb{I}_i \subset \mathbb{J}_\lambda$ so that $\cup_i \mathbb{I}_i = \mathbb{J}^\lambda$.

Output: An approximate solution \underline{x}

```

x := 0
α := 0                                ▷ initialize approximate solution
r := b - Mx
for all  $\mathbb{I}_i$  do                        ▷ Loop over Schwarz blocks...
    x := x + PMG(r,  $\underline{k}_{\text{lo}}$ ,  $\mathbb{I}_i$ )      ▷ solve block no.  $i$ 
    α := α +  $\chi_{m(\mathbb{I}_i, -, -, -)}$ 
end for
x := x./α                            ▷ Apply scaling in overlap regions

```

Within the scope of this work, the additive Schwarz solver is used as a smoother for the multigrid method. As such, we introduced a minor modification to the original formulation: in the last line of Algorithm 12, the solution is divided by the number of blocks which contain a specific cell. This damping of the approximate solution in the overlapping regions has shown to improve the number of iterations when $\text{Swz}(-)$ is used as a smoother for the multigrid method (Algorithm 14).

A multigrid algorithm based on orthonormalization. Experiments have shown that the classic multigrid algorithm, as could be found e.g. in the textbook of Saad [28] often diverges for DG and XDG methods. To overcome this issue, we employ a residual minimization approach: Let $\underline{Z} = (z_1, \dots, z_l) \in \mathbb{R}^{L \times l}$ be a family of approximate solutions, e.g. from some Additive Schwarz or from a coarse grid solver. Furthermore let be $\underline{W} = (w_1, \dots, w_l) = \underline{M} \underline{Z} \in \mathbb{R}^{L \times l}$ be the image of \underline{Z} under the application of \underline{M} . For the residual-optimized solution, one employs the Ansatz

$$\underline{x} = \underline{x}_0 + \sum_i \alpha_i z_i, \quad (38)$$

in order to minimize the 2-norm of the residual

$$\underline{r} := \underline{b} - \underline{M} \underline{x} \quad (39)$$

$$= \underline{r}_0 - \underline{M} \underline{Z} \underline{\alpha} \quad (40)$$

$$= \underline{r}_0 - \underline{W} \underline{\alpha}. \quad (41)$$

As widely known, the coefficients $\underline{\alpha}$ at which $|\underline{r}|_2$ becomes minimal are determined by the system

$$(\underline{W}^T \cdot \underline{W}) \underline{\alpha} = \underline{W}^T \cdot \underline{r}_0. \quad (42)$$

Furthermore, if columns of \underline{W} are orthonormal, the left-hand-side of equation (42) becomes identity. This can be achieved through a Gram-Schmidt algorithm, which is used in the following residual minimization algorithm which is the foundation of our modified multigrid method:

Algorithm 13 (Residual minimization). $(\underline{x}, \underline{r}) = \text{RM}(\underline{x}_0, \underline{z}, \underline{W}, \underline{Z})$ is computed as follows:

Input: A solution-guess $\underline{z} \in \mathbb{R}^L$, e.g. from some pre-conditioner. An orthonormal system $\underline{W} = (\underline{w}_1, \dots, \underline{w}_l) \in \mathbb{R}^{L \times l}$ and its application onto the system matrix \underline{Z} , i.e. $\underline{W} = \underline{M}\underline{Z}$. Note that $l = 0$ is allowed, i.e. \underline{W} and \underline{Z} can be empty.

Output: An approximate solution \underline{x} whose residual \underline{r} is not greater in the l_2 -norm than the residual of the initial value \underline{x}_0 . Furthermore, updated $\underline{W}, \underline{Z} \in \mathbb{R}^{L \times l+1}$ where the columns of \underline{W} are orthonormal and $\underline{W} = \underline{M}\underline{Z}$.

$$\underline{r}_0 = \underline{b} - \underline{M}\underline{x}_0$$

$$\underline{w}_{l+1} = \underline{M}\underline{z}$$

for all columns \underline{w}_i of \underline{W} **do**

▷ Gram-Schmidt loop...

$$\beta := \underline{w}_i \cdot \underline{w}_{l+1}$$

$$\underline{w}_{l+1} := \underline{w}_{l+1} - \beta \underline{w}_i$$

$$\underline{z} := \underline{z} - \beta \underline{Z}_i$$

end for

$$\gamma := 1/|\underline{w}_{l+1}|_2, \underline{w}_{l+1} := \gamma \underline{w}_{l+1}, \underline{z}_{l+1} := \gamma \underline{z}_{l+1}$$

$$\underline{W} := (\underline{W}, \underline{w}_{l+1}), \underline{Z} := (\underline{Z}, \underline{z})$$

▷ Store vectors \underline{w}_{l+1} and \underline{z}

$$\alpha_{l+1} := \underline{w}_{l+1} \cdot \underline{r}_0, \underline{\alpha} := (\underline{\alpha}, \alpha_{l+1})$$

$$\underline{x} := \underline{x}_0 + \underline{Z} \cdot \underline{\alpha}$$

▷ optimized solution

$$\underline{r} := \underline{r}_0 - \underline{W} \cdot \underline{\alpha}$$

▷ residual for optimized solution

In order to define a multigrid algorithm, one employs the restriction matrix $\underline{R}^{X,\lambda} \in \mathbb{R}^{L \times L_c}$ introduced in Eq. (34). from which one infers the

restricted-system matrix $\underline{\underline{M}}^{\lambda+1}$, cf. Eq. (37). Here, L_c denotes the vector-space dimension of the coarser space $\mathbb{V}_k^{X,\lambda+1}$ at mesh level $\lambda + 1$. As noted, the classical multigrid algorithm very often does not converge for DG or XDG methods, at least if Block-Jacobi or Schwarz algorithms are used as smoothers. Therefore, we employ $\text{RM}(\dots)$ after each pre- and post-smoother step and after the coarse-grid correction in order to ensure a non-increasing residual norm.

Algorithm 14 (Orthonormalization multigrid). $(\underline{x}, \underline{r}) = \text{MG}(\underline{x}_0, \underline{b}, \underline{\underline{M}})$ is computed as follows:

Input: A right-hand-side \underline{b} and an initial solution guess \underline{x}_0 (can be zero).

Output: An approximate solution \underline{x} whose residual norm is less than or equal to the residual norm of the initial guess \underline{x}_0 .

```

 $\underline{Z} := ()$ ,  $\underline{W} := ()$  ▷ Initialize as empty
 $\underline{r}_0 := \underline{b} - \underline{\underline{M}}\underline{x}_0$ ,  $\underline{r} := \underline{r}_0$ ,  $\underline{x} := \underline{x}_0$  ▷ residual of interstitial solution
while  $|\underline{r}|_2 > \varepsilon$  do
     $\underline{z} := \text{Swz}(\underline{b})$  ▷ pre-smoother
     $(\underline{x}, \underline{r}) = \text{RM}(\underline{x}_0, \underline{z}, \underline{W}, \underline{Z})$  ▷ minimize residual of pre-smoother
     $\underline{r}_c := (\underline{R}^{X,\lambda})^T \underline{r}$  ▷ restrict residual
     $(\underline{z}_c, \underline{r}_c) = \text{MG}(0, \underline{r}_c, \underline{\underline{M}}^{\lambda+1})$  ▷ call multigrid on coarser level
     $\underline{z} := \underline{R}^{X,\lambda} \underline{z}_c$  ▷ prolongate coarse-grid correction
     $(\underline{x}, \underline{r}) = \text{RM}(\underline{x}_0, \underline{z}, \underline{W}, \underline{Z})$  ▷ minimize residual
     $\underline{z} := \text{Swz}(\underline{b})$  ▷ pre-smoother
     $(\underline{x}, \underline{r}) = \text{RM}(\underline{x}_0, \underline{z}, \underline{W}, \underline{Z})$  ▷ minimize residual of pre-smoother
end while

```

4. Solver Performance studies

The performance of solvers introduced in section 3.3 is investigated for the XDG Poisson problem (2) on the domain $\Omega = (-1, 1)^3$ with homogeneous Dirichlet boundary conditions ($\Gamma_D = \partial\Omega$, $g_{\text{Diri}} = 0$), right hand side $f = 1$ and a large ratio of diffusion coefficients ($\mu_{\mathfrak{A}} = 1$, $\mu_{\mathfrak{B}} = 1000$) for a Level-Set $\varphi = x^2 + y^2 + z^3 - (7/10)^2$. Equidistant, Cartesian meshes were employed with a resolution of 2^3 , 4^3 , 8^3 , etc., cells and polynomial degrees k of 2, 3 and 5. The agglomeration threshold α (cf. section 2.3) is set 0.1 for $k = 2, 3$ and 0.3 for $k = 5$. Details on degrees-of-freedom can be found in Table 1. All solvers were configured to terminate if the 2-norm of residual is below 10^{-10} .

In order to assess runtime-measurements, one first has to ensure that the subroutines of which the iterative solvers are composed of. The most complex of those is the sparse matrix-vector and matrix-matrix product. A (non-systematic) comparison against MATLAB shows that the implementations in BoSSS are quite decent, as can be seen in Table 2. The test matrix for this benchmark is the XDG system used in this section, for 6^3 cells and a polynomial order $k = 5$, yielding a matrix with 24,192 non-zero rows. It should be noted that the BoSSS implementation exploits the block-structure of the XDG matrix, thus BLAS (Intel MKL 11.0) subroutines can be used for the inner dense matrix-matrix and matrix-vector products. Since BoSSS is MPI parallel, only the sequential version of the MKL is used in order to avoid that all MPI ranks try to use all cores of some compute node.

Results of run-time measurements can be seen in Figure 3. A performance base-line is given by the runtime of the (direct sparse) PARDISO solver [29, 30, 31]. As expected, direct sparse solvers are superior for comparatively small problems up to 100,000 degrees-of-freedom. In addition to the presented results, we also tested the MUMPS package [32, 33], showing only minor differences in runtime behavior, which are therefore skipped. Despite having a symmetric, positive definite system the direct solver was configured to assume general matrices, since we are finally interested in non-symmetric systems such as the Navier-Stokes problem (4). Beyond 100,000 degrees-of-freedom, iterative solvers out-perform sparse direct systems and show a linear run-time behavior, with one exception.

Runtime-measurements also include setup-costs for the iterative solvers. Figures 5 and 4 outline runtime details for the orthonormalization multigrid (Algorithm 14) as well as GMRES with p-multigrid preconditioner (Algorithm 11), respectively. As individual solver phases, we identify (i) the setup of the XDG aggregation grid basis, including the re-orthonormalization in cut-cells (matrix \underline{S}^λ , cf. Eq. 33), (ii) the sparse matrix-matrix products required to setup the sequence of linear systems (cf. Eq. 37) and (iii) the iterative procedure itself.

A clearly negative result here is the worse-than-linear runtime behavior for the orthonormalization multigrid for $k = 5$, cf. Figure 3. While this is caused by the solver iterations (cf. Figure 5), the number of iterations is fairly constant for the number of degrees-of-freedom. In order to achieve this, the separation degree k_{lo} (cf. Algorithm 11) had to be increased from 1 for the cases $k = 2, 3$ to 3 for the case $k = 5$. This hints (and is also verified by measurements) that the time for a single iteration is dominated by calls to

	grid resolution							
	2^3	4^3	8^3	16^3	24^3	32^3	48^3	64^3
$p = 2$	160	880	5920	43840	145200	339040	1134560	2671600
$p = 3$	320	1760	11840	87680	290400	678080	2269120	
$p = 5$	896	4928	33152	245504	813120			

Table 1: degrees of freedom in dependency of grid resolution and polynomial-degree k for the subsequent Performance plots shown in figure 3, 6, 4 and 5 for the problem described in section 4

	matrix-matrix		
	BoSSS 1 MPI core	BoSSS 4 MPI cores	Matlab OpenMP
i7 6700HQ (4 cores)	3.88	1.293	5.19
Xeon E5-2630L v4 (20 cores)	5.86	1.687	4.42

	matrix-vector		
	i7 6700HQ (4 cores)	$14.6 \cdot 10^{-3}$	$8.99 \cdot 10^{-3}$
Xeon E5-2630L v4 (20 cores)	$29.2 \cdot 10^{-3}$	$9.14 \cdot 10^{-3}$	$7.53 \cdot 10^{-3}$

Table 2: Runtime (in seconds) of a sparse matrix-matrix and matrix-vector multiplication in BoSSS vs. MATLAB on two different computer systems for a quadratic matrix with 24,192 non-zero rows. This verifies that these building blocks provide decent performance, given that the BoSSS implementation is sequential (within each MPI core) and MATLAB is OpenMP parallel. An advantage of the BoSSS implementation is that it exploits the block-structure of the XDG matrix, which is not known to MATLAB.

the sparse linear solver for the low-order Schwarz blocks. We want to point out that such a behavior could not be observed using a standard DG method - there, $k_{lo} = 1$ seems to be sufficient, with only a minor dependence of the number of iterations on k . Ongoing works investigate an adaptation of k_{lo} in cut-cells, in order to regain the runtime behavior for DG problems for XDG.

5. Conclusion and Outlook

In this work, the XDG framework available in BoSSS for the discretization of PDEs with discontinuous coefficients was presented. and a unified notation for the agglomeration of small cut-cells and aggregation multigrid was devel-

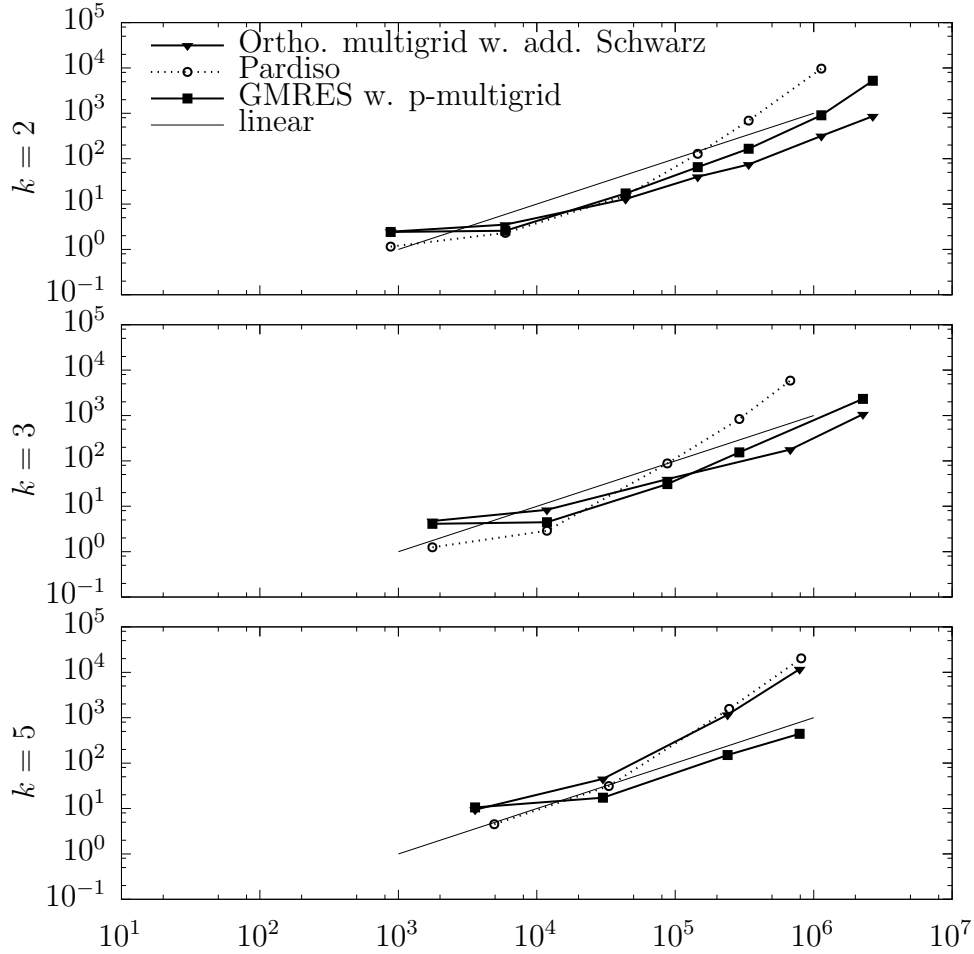


Figure 3: Overall solver runtime (in seconds) versus. degrees-of-freedom, for different polynomial degrees k , for the XDG Poisson problem with 1:1000 diffusion coefficient ratio. The solver are: PARDISO, orthonormalization multigrid (alg. 14), GMRES with p-multigrid (alg. 11).

oped. The practical advantages of XDG for single phase flows is the elimination of the meshing process, which is especially useful for time-evolving geometries. Regarding two-, resp. multiphase flows, the XDG method preserves the h^{k+1} -convergence rate despite the presence of discontinuous material coefficients, cf. [24, 2].

Furthermore, in this work we presented a combined p- and h-multigrid method and assessed its performance. Although the BoSSS code is fully MPI

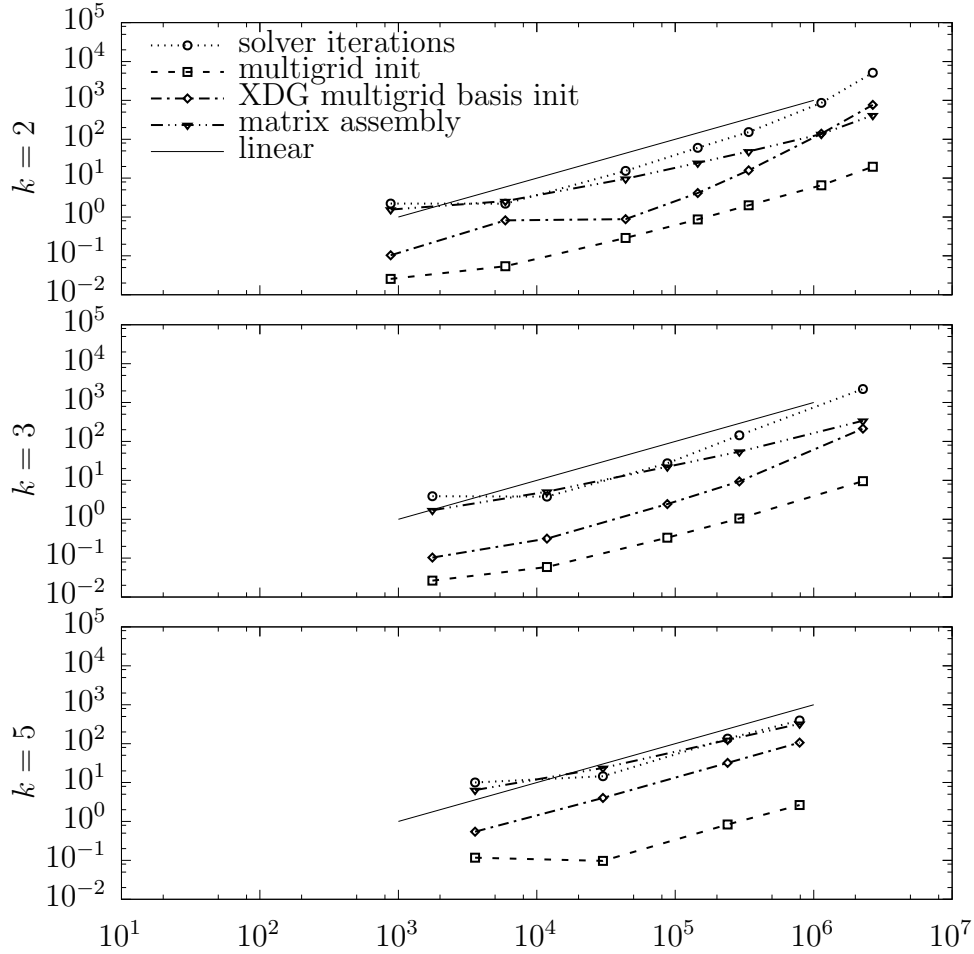


Figure 4: Runtime (in seconds) of individual solver phases of the GMRES with p-multigrid (alg. 11) versus degrees-of-freedom for different polynomial degrees k , for the XDG Poisson problem with 1:1000 diffusion coefficient ratio. Note that the matrix assembly is not counted as part of the solution process and is only given for purpose additional perspective.

parallel, up to this point, parallel scaling has not been investigated *systematically* and only set of various results such as Table 2 exist. Extensive tests for parallel efficiency of the presented solvers and other subsystems of BoSSS are a matter of ongoing work and will be published in the BoSSS handbook, available at the online code repository at Github.

So far, only the solution of linear systems was addressed. Newton-methods for the nonlinear Navier-Stokes problem (4) coupled together with the Level-

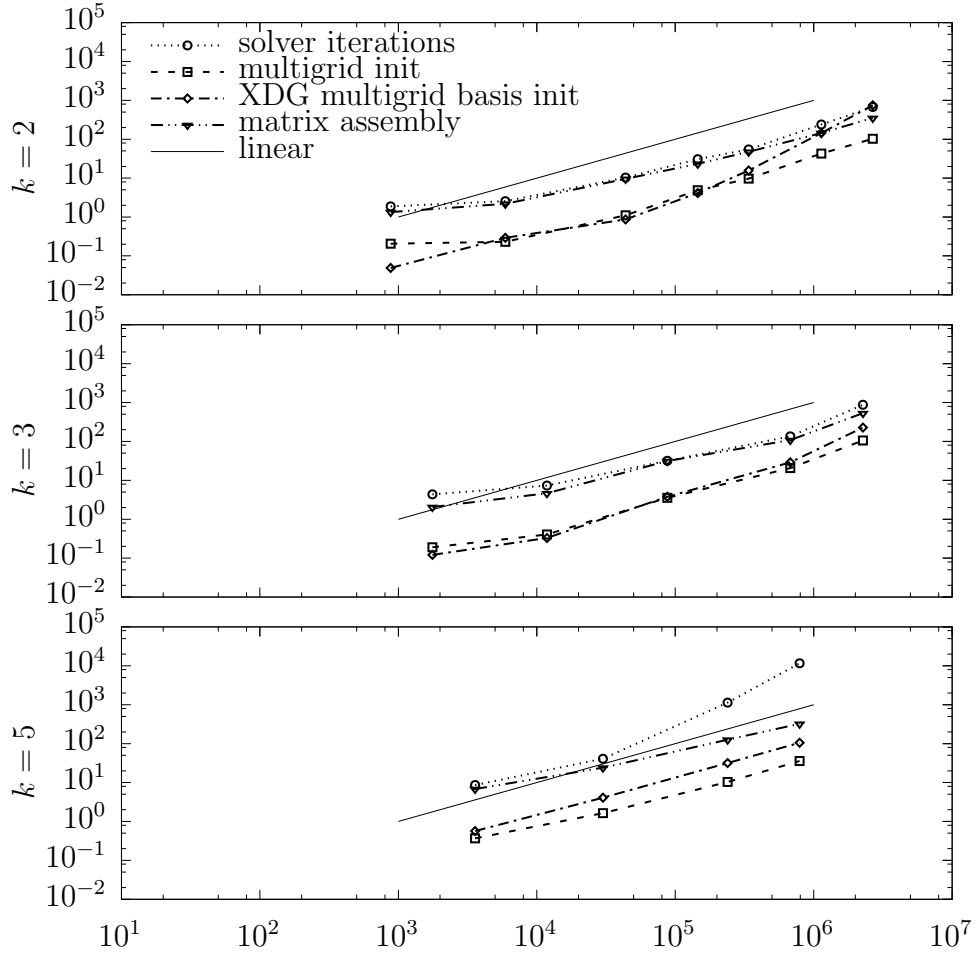


Figure 5: Runtime (in seconds) of individual solver phases of the orthonormalization multigrid (alg. 14) versus degrees-of-freedom for different polynomial degrees k , for the XDG Poisson problem with 1:1000 diffusion coefficient ratio. Note that the matrix assembly is not counted as part of the solution process and is only given for purpose additional perspective.

Set evolution (9) are subject of ongoing works and will be the issue of upcoming publications.

Acknowledgment

The work of F. Kummer and M. Smuda is supported by the German Science Foundation (DFG) through the Collaborative Research Centre (SFB)

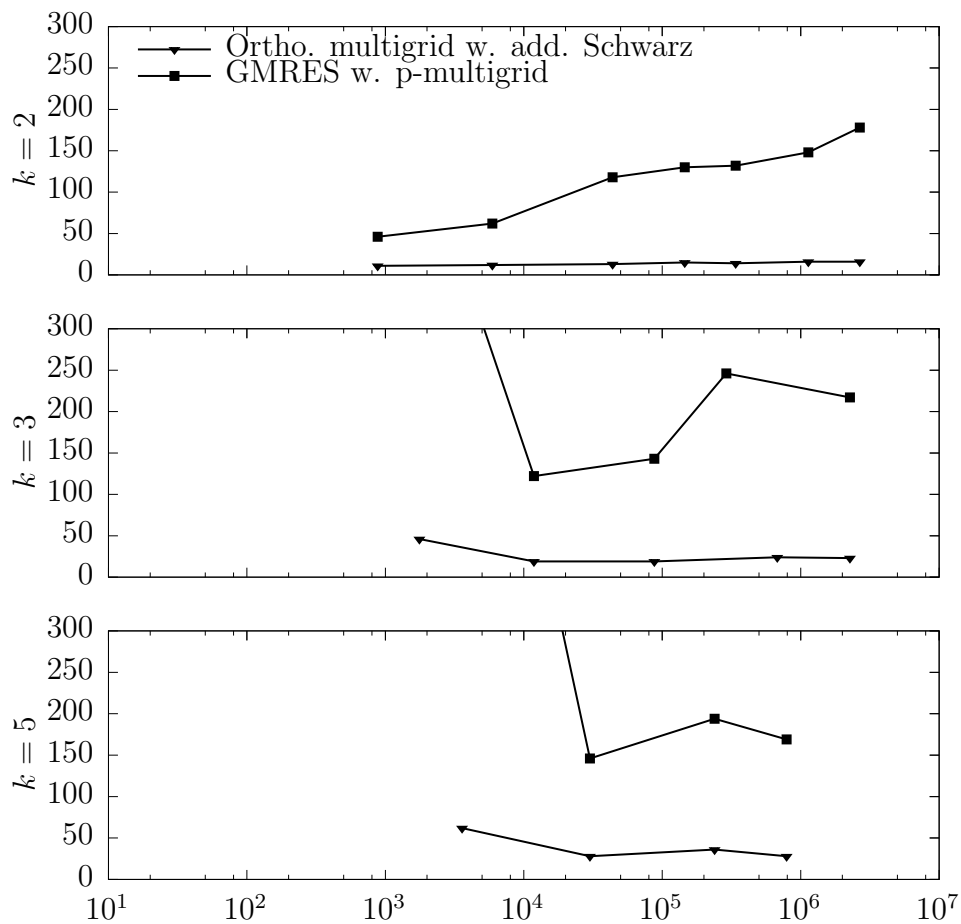


Figure 6: Number of iterations versus degrees-of-freedom for different polynomial degrees k for the XDG Poisson problem with 1:1000 diffusion coefficient ratio. The number of iterations for the orthonormalization multigrid is nearly independent from the number of degrees-of-freedom. GMRES with a single level of p-multigrid shows a slight increase of iterations with outliers at the lower end, where direct solvers are superior. Despite the higher number of iterations, GMRES might still be faster in wall-clock time cf. Figure 3.

1194 “Interaction between Transport and Wetting Processes”.

References

- [1] D. Krause, F. Kummer, An incompressible immersed boundary solver for moving body flows using a cut cell discontinuous Galerkin method,

Computers & Fluids 153 (2017) 118–129. doi:10.1016/j.compfluid.2017.05.008.

- [2] B. Müller, S. Krämer-Eis, F. Kummer, M. Oberlack, A high-order discontinuous Galerkin method for compressible flows with immersed boundaries, *International Journal for Numerical Methods in Engineering* 110 (1) (2017) 3–30. doi:10.1002/nme.5343.
- [3] W. H. Reed, T. R. Hill, Triangular mesh methods for the neutron transport equation, in: *National topical meeting on mathematical models and computational techniques for analysis of nuclear systems*, CONF-7304142; LA-UR73-479, Los Alamos Scientific Lab., N.Mex. (USA), 1973, p. 23.
- [4] B. Cockburn, C.-W. Shu, The P1-RKDG method for two-dimensional Euler equations of gas dynamics, *Tech. Rep. ICASE Report 91-32*, NASA Langley Research Center, Hampton, Virginia 23665-5225, USA (1991).
- [5] D. N. Arnold, An interior penalty finite element method with discontinuous elements, *SIAM Journal on Numerical Analysis* 19 (4) (1982) 742. doi:10.1137/0719052.
- [6] I. Babuška, The finite element method for elliptic equations with discontinuous coefficients, *Computing* 5 (3) (1970) 207–213. doi:10.1007/BF02248021.
- [7] J. W. Barrett, C. M. Elliott, Fitted and unfitted finite-element methods for elliptic equations with Smooth interfaces, *IMA Journal of Numerical Analysis* 7 (3) (1987) 283–300. doi:10.1093/imanum/7.3.283.
- [8] N. Moës, J. Dolbow, T. Belytschko, A finite element method for crack growth without remeshing, *International Journal for Numerical Methods in Engineering* 46 (1999) 131–150. doi:10.1002/(SICI)1097-0207(19990910)46:1<131::AID-NME726>3.0.CO;2-J.
- [9] J. Chessa, T. Belytschko, Arbitrary discontinuities in space-time finite elements by level sets and X-FEM, *International Journal for Numerical Methods in Engineering* 61 (15) (2004) 2595–2614. doi:10.1002/nme.1155.

- [10] S. Groß, A. Reusken, An extended pressure finite element space for two-phase incompressible flows with surface tension, *Journal of Computational Physics* 224 (1) (2007) 40–58. doi:10.1016/j.jcp.2006.12.021.
- [11] S. Groß, A. Reusken, Finite element discretization error analysis of a surface tension force in two-phase incompressible flows, *SIAM Journal on Numerical Analysis* 45 (4) (2007) 1679–1700. doi:10.1137/060667530.
- [12] T. P. Fries, The intrinsic XFEM for two-fluid flows, *International Journal for Numerical Methods in Fluids* 60 (4) (2009) 437–471. doi:10.1002/flid.1901.
- [13] K.-W. Cheng, T.-P. Fries, XFEM with hanging nodes for two-phase incompressible flow, *Computer Methods in Applied Mechanics and Engineering* 245-246 (2012) 290–312. doi:10.1016/j.cma.2012.07.011.
- [14] H. Sauerland, T.-P. Fries, The stable XFEM for two-phase flows, *Computers & Fluids* 87 (2013) 41–49. doi:10.1016/j.compfluid.2012.10.017.
- [15] P. Bastian, C. Engwer, An unfitted finite element method using discontinuous Galerkin, *International Journal for Numerical Methods in Engineering* 79 (12) (2009) 1557–1576. doi:10.1002/nme.2631.
- [16] F. Heimann, C. Engwer, O. Ippisch, P. Bastian, An unfitted interior penalty discontinuous Galerkin method for incompressible Navier-Stokes two-phase flow, *International Journal for Numerical Methods in Fluids* 71 (3) (2013) 269–293. doi:10.1002/flid.3653.
- [17] D. A. Di Pietro, A. Ern, *Mathematical Aspects of Discontinuous Galerkin Methods*, no. 69 in *Mathématiques et Applications*, Springer, 2011.
- [18] J. S. Hesthaven, T. Warburton, *Nodal Discontinuous Galerkin Methods: Algorithms, Analysis, and Applications*, no. 54 in *Texts in Applied Mathematics*, Springer-Verlag, 2008.
- [19] B. Müller, F. Kummer, M. Oberlack, Highly accurate surface and volume integration on implicit domains by means of moment-fitting, *International Journal for Numerical Methods in Engineering* 96 (8) (2013) 512–528. doi:10.1002/nme.4569.

- [20] R. I. Saye, High-order quadrature methods for implicitly defined surface and volumes in hyperrectangles, *SIAM Journal on Scientific Computing* 37 (2) (2015) A993–A1019. doi:10.1137/140966290.
- [21] F. Kummer, T. Warburton, Patch-recovery filters for curvature in discontinuous Galerkin-based level-set methods, *Communications in Computational Physics* 19 (02) (2016) 329–353. doi:10.4208/cicp.191114.140715a.
- [22] K. Hillewaert, Development of the discontinuous Galerkin method for high-resolution, large scale CFD and acoustics in industrial geometries, PhD thesis, Université catholique de Louvain, Louvain-la-Neuve, Belgium (2013).
- [23] V. Girault, B. Riviere, M. F. Wheeler, A discontinuous Galerkin method with nonoverlapping domain decomposition for the Stokes and Navier-Stokes problems, *Math. Comp* 74 (249) (2005) 53–84.
- [24] F. Kummer, Extended discontinuous Galerkin methods for two-phase flows: the spatial discretization, *International Journal for Numerical Methods in Engineering* 109 (2) (2017) 259–289. doi:10.1002/nme.5288.
- [25] F. Kummer, B. Müller, T. Utz, Time integration for extended discontinuous Galerkin methods with moving domains, *International Journal for Numerical Methods in Engineering* (2017). doi:10.1002/nme.5634.
- [26] M. J. Gander, Schwartz methods over the course of time, *ETNA. Electronic Transactions on Numerical Analysis* [electronic only] 31 (2008) 228–255.
- [27] G. Karypis, V. Kumar, A fast and high quality multilevel scheme for partitioning irregular graphs, *SIAM Journal on Scientific Computing* 20 (1) (1998) 359–392. doi:10.1137/S1064827595287997.
- [28] Y. Saad, *Iterative methods for sparse linear systems*, 2nd Edition, SIAM, Philadelphia, 2003.
- [29] O. Schenk, Two-level dynamic scheduling in PARDISO: improved scalability on shared memory multiprocessing systems, *Parallel Computing* 28 (2) (2002) 187–197. doi:10.1016/S0167-8191(01)00135-1.

- [30] O. Schenk, Solving unsymmetric sparse systems of linear equations with PARDISO, *Future Generation Computer Systems* 20 (3) (2004) 475–487. doi:10.1016/j.future.2003.07.011.
- [31] O. Schenk, K. Gärtner, On fast factorization pivoting methods for sparse symmetric indefinite systems, *Electronic Transactions on Numerical Analysis* 23 (2006) 158–179.
- [32] P. R. Amestoy, I. S. Duff, J. Koster, J.-Y. L'Excellent, A fully asynchronous multifrontal solver using distributed dynamic scheduling, *SIAM Journal on Matrix Analysis and Applications* 23 (1) (2001) 15–41.
- [33] P. R. Amestoy, A. Guermouche, J.-Y. L'Excellent, S. Pralet, Hybrid scheduling for the parallel solution of linear systems, *Parallel Computing* 32 (2) (2006) 136–156.